View metadata, citation and similar papers at core.ac.uk

brought to you by CORE

provided by Digital.CSIC

Non-adiabatic couplings and dynamics in proton transfer reactions of Hn+ systems: Application to H2+H2+→H+H3+ collisions

Cristina Sanz-Sanz, Alfredo Aguado, Octavio Roncero, and Fedor Naumkin

Citation: The Journal of Chemical Physics **143**, 234303 (2015); doi: 10.1063/1.4937138

View online: http://dx.doi.org/10.1063/1.4937138

View Table of Contents: http://scitation.aip.org/content/aip/journal/jcp/143/23?ver=pdfcov

Published by the AIP Publishing

Articles you may be interested in

Radiative charge transfer in He+ + H2 collisions in the milli- to nano-electron-volt range: A theoretical study within state-to-state and optical potential approaches
J. Chem. Phys. **138**, 104315 (2013); 10.1063/1.4793986

Nuclear spin dependence of the reaction of H 3 + with H2. I. Kinetics and modeling
J. Chem. Phys. **134**, 194310 (2011); 10.1063/1.3587245

Influence of nuclear exchange on nonadiabatic electron processes in H + +H 2 collisions
J. Chem. Phys. **133**, 244307 (2010); 10.1063/1.3518417

A time-dependent wave packet quantum scattering study of the reaction H D + (v = 0 – 3 ; j 0 = 1) + He → He H + (He D +) + D (H)
J. Chem. Phys. **127**, 164318 (2007); 10.1063/1.2800009

Exact quantum dynamics study of the O + + H 2 (v = 0 , j = 0) → O H + + H ion-molecule reaction and comparison with quasiclassical trajectory calculations
J. Chem. Phys. **124**, 144301 (2006); 10.1063/1.2179429

Reuse of AIP Publishing content is subject to the terms: https://publishing.aip.org/authors/rights-and-permissions. Downloaded to IP: 161.111.22.69 On: Thu, 04 Aug 2016 09:50:28

Non-adiabatic couplings and dynamics in proton transfer reactions of H_n^+ systems: Application to $H_2 + H_2^+ \rightarrow H + H_3^+$ collisions

Cristina Sanz-Sanz,[1] Alfredo Aguado,[1] Octavio Roncero,[2,a)] and Fedor Naumkin[3,b)]
[1]*Departamento de Química Física Aplicada (UAM), Unidad Asociada IFF-CSIC, Facultad de Ciencias C-XIV, Universidad Autónoma de Madrid, 28049 Madrid, Spain*
[2]*Instituto de Física Fundamental, CSIC, C/ Serrano, 123, 28006 Madrid, Spain*
[3]*Faculty of Science, UOIT, Oshawa, Ontario L1H 7K4, Canada*

(Received 7 October 2015; accepted 23 November 2015; published online 17 December 2015)

Analytical derivatives and non-adiabatic coupling matrix elements are derived for H_n^+ systems (n = 3–5). The method uses a generalized Hellmann-Feynman theorem applied to a multi-state description based on diatomics-in-molecules (for H_3^+) or triatomics-in-molecules (for H_4^+ and H_5^+) formalisms, corrected with a permutationally invariant many-body term to get high accuracy. The analytical non-adiabatic coupling matrix elements are compared with *ab initio* calculations performed at multi-reference configuration interaction level. These magnitudes are used to calculate $H_2(v' = 0, j' = 0) + H_2^+(v, j = 0)$ collisions, to determine the effect of electronic transitions using a molecular dynamics method with electronic transitions. Cross sections for several initial vibrational states of H_2^+ are calculated and compared with the available experimental data, yielding an excellent agreement. The effect of vibrational excitation of H_2^+ reactant and its relation with non-adiabatic processes are discussed. Also, the behavior at low collisional energies, in the 1 meV-0.1 eV interval, of interest in astrophysical environments, is discussed in terms of the long range behaviour of the interaction potential which is properly described within the triatomics-in-molecules formalism. © *2015 AIP Publishing LLC*. [http://dx.doi.org/10.1063/1.4937138]

I. INTRODUCTION

In the interstellar medium (ISM), hydrogen is by far the most abundant atom. H_2 is the most abundant molecule and is formed on the surface of dust particles by successive adsorption of H atoms[1] and several gas phase processes such as radiative association of H atoms. Another gas phase reaction of interest is

$$H + H_2^+ \rightarrow H_2 + H^+, \quad (1)$$

which is important in the formation of H_2 in the early universe. Once H_2 is formed, the chemistry in space starts by the formation of the first hydrides. In cold clouds, the most abundant ion is H_3^+ which is formed in the collision

$$H_2 + H_2^+ \rightarrow H_3^+ + H, \quad (2)$$

which is exothermic by 1.2 eV and therefore very efficient. This explains why H_2^+, formed by the ionization of H_2 by cosmic rays, is not very abundant. On the contrary, when H_3^+ collides with molecular hydrogen, a proton exchange is produced as

$$H_2 + H_3^+ \rightarrow H_3^+ + H_2, \quad (3)$$

which does not destroy H_3^+, but simply transforms it. This last reaction is the main source of ortho/para-conversion of H_3^+ and when involving deuterium is the main source of deuterated H_3^+.

H_3^+ is involved in many processes in astrochemistry with other atoms and polyatomic molecules, electrons and hydrogen, and protons and H^-. These processes are described in details in many review articles such as Refs. 2–6 and there are special issues devoted to H_3^+.[7] Many of these processes are very efficient because they are highly exothermic. In cold molecular clouds, many reactive species are adsorbed on icy particles, and the densities of electrons and cosmic rays are considerably reduced, making possible slow processes such as deuteration through Eq. (3) exchange reaction. Deuterated species are favored by their lower zero-point energy (ZPE), thus shifting the equilibrium in gas phase reactions such as that of Eq. (3).[8,9] H_3^+, as the universal protonator,[2,10–12] plays a central role in the interstellar chemistry, since it is at the origin of the formation of the first hydrides, including deuterated species.

In the reactive cycle of pure hydrogen species of Eqs. (1)–(3), there are several electronic states, corresponding to electron holes in each of the equivalent hydrogen atoms. This makes necessary to use a multi-state description of the potential energy surfaces (PESs), such as the diatomics-in-molecules (DIM) frequently used to describe these systems.[13–16] The DIM description is however not enough to describe accurately H_3^+ fragments, and several many-body (MB) terms have to be added. For H_3^+, this was done for ground singlet[17] and triplet[18] states by adding a three-body term to the DIM PES so that an accuracy of about 1-5 cm^{-1} was reached on global surfaces designed to describe the reactive collisions. This was later improved by adding the long range (LR) terms, charge-induced dipole and charge-quadrupole, on the diagonal

a)Electronic address: octavio.roncero@csic.es
b)On sabbatical at IFF-CSIC.

 © 2015 AIP Publishing LLC

Reuse of AIP Publishing content is subject to the terms: https://publishing.aip.org/authors/rights-and-permissions. Downloaded to IP: 161.111.22.69 On: Thu, 04 Aug 2016 09:50:28

terms of the DIM Hamiltonian matrix.[19] Another approach was adopted adding three-body terms on the non-diagonal matrix elements of the DIM matrix.[20]

For H_4^+ and H_5^+, the DIM approach does not describe the different fragmentation channels because many of them correspond to triatomic H_3^+. In order to describe these channels, a generalization of the DIM approach was used, the triatomics-in-molecules (TRIM) approach, which is essentially exact at the asymptotes but not in the interaction region. To get the desired accuracy, many-body terms were added to describe the ground state. With this approach, accurate 6 and 9 dimension PESs were obtained for H_4^+ [21] and H_5^+.[22]

In this work, we generalize these approaches to describe several electronic states of H_n^+, with special emphasis on analytic non-adiabatic coupling matrix elements (NACMEs) and potential derivatives, using the generalized Hellmann-Feynman theorem. The analytical derivatives of the ground PES are tested with quasi-classical trajectories (QCTs) on $H_2 + H^+$, $H_2 + H_2^+$, and $H_2 + H_3^+$ reactive collisions, getting a significant speedup and better accuracy as compared to the numerical ones previously used for H_3^+ [23,24] and H_5^+.[25] For H_3^+,[23,24] with a deep insertion well, the reaction mechanism is essentially statistical, and QCTs underestimate the cross section because this method is unable to describe tunneling for high total angular momenta. For H_5^+, the exchange reaction of Eq. (3) has been treated with statistical approaches,[26–28] using asymptotic long range interaction potentials between reactants. When considering the full potential of Ref. 22 and a dynamical bias in the statistical model, it was found that the complex formation can only occur at low temperatures, while for $T > 10$ K, a direct proton hop mechanism dominates.[25]

In this work, we focus on the non-adiabatic dynamic of the reaction of Eq. (2) using the classical molecular dynamics with quantum transitions (MDQTs) of Tully.[29] The MDQT is a variant of the commonly known surface hopping applied to study the non-adiabatic reactive $H^+ + H_2$ collisions by Krenos *et al.*[30] and supported by the experiments of Ochs and Teloy.[31] In this reaction, there is a curve crossing in the entrance channel very close to the ZPE of the reactants, and here, we shall analyze the effect of non-adiabatic transitions as a function of translational energy and vibrational excitation of the H_2^+ reactants. The results are compared with the available experimental data[30,32–35] and with the previous surface hopping results.[30,36,37] These last results were obtained with DIM PESs,[38] which do not include long-range interaction terms and are not accurate to describe H_3^+ fragments. In the present approach, these two problems are solved.

The organization of the paper is as follows. In Section II, the theoretical methods used are presented: the generalized Hellmann-Feynman approach used to obtain analytical potential derivatives and non-adiabatic matrix elements applied to the TRIM+many body (TRIM+MB) method. Also, some details of the numerical implementation of the MDQT developed in this work will be briefly described. In Section III, the results obtained for the reaction of Eq. (2) will be shown and discussed. Finally, Section IV is devoted to extract some conclusions.

II. THEORETICAL METHODS

A. Generalized Hellmann-Feynman theorem

We will consider N adiabatic eigenstates, ϕ_n^a, which are obtained as solution of the electronic Schrödinger equations

$$H(\mathbf{R})\phi_n^a = W_n(\mathbf{R})\phi_n^a, \tag{4}$$

where W_n is the electronic eigenvalue at a nuclear configuration given by the nuclear coordinates $\mathbf{R}$. These eigenfunctions are represented in a basis set, φ_m, as

$$\phi_n^a = \sum_m T_n^m \varphi_m^d. \tag{5}$$

This basis set, hereafter called diabatic, does not depend on the nuclear configuration $\mathbf{R}$ and is assumed to be complete and orthonormal. The procedure can be easily generalized to the non-orthonormal case. In this diabatic basis, the Hamiltonian operator H takes a matricial form of elements $H_{mm'}$.

Differentiating Eq. (4) with respect to $\alpha \equiv \mathbf{R}_\alpha$, a component of the hypervector determining the nuclear configuration,

$$\frac{\partial H}{\partial \alpha}\phi_n + H\frac{\partial \phi_n}{\partial \alpha} = \frac{\partial W_n}{\partial \alpha}\phi_n + W_n\frac{\partial \phi_n}{\partial \alpha}, \tag{6}$$

and premultiplying by $\phi_{n'}$ and integrating over electronic coordinates, a generalized version of the Hellmann-Feynman theorem is obtained as

$$\left\langle \phi_{n'} \left| \frac{\partial H}{\partial \alpha} \right| \phi_n \right\rangle = (W_n - W_{n'}) \left\langle \phi_{n'} \left| \frac{\partial}{\partial \alpha} \right| \phi_n \right\rangle + \delta_{nn'}\frac{\partial W_n}{\partial \alpha}, \tag{7}$$

where the NACMEs, $\langle \phi_{n'} | \frac{\partial}{\partial \alpha} | \phi_n \rangle$, are non-diagonal.

To evaluate the derivatives of the electronic Hamiltonian it is convenient to represent the adiabatic eigenfunctions in the diabatic basis, so that using $\partial \varphi_m^d / \partial \alpha = 0$, two cases can be distinguished as the following:

1. Diagonal with $n = n'$, in which NACMEs are zero, giving the derivative of the adiabatic potential as

$$\frac{\partial W_n}{\partial \alpha} = \sum_{mm'} \left(T_n^{m'}\right)^\dagger T_n^m \frac{\partial H_{m'm}}{\partial \alpha}. \tag{8}$$

   An equivalent formalism was previously employed, in particular, for obtaining derivatives of DIM potential energy surfaces of Rg_n^+ (Rg = He, Ne, Ar) and Ar_n^*,[39–43] used further for their geometry optimizations.
2. Non-diagonal with $n \neq n'$, to evaluate the NACME as

$$\left\langle \phi_{n'} \left| \frac{\partial}{\partial \alpha} \right| \phi_n \right\rangle = d_{n'n}^\alpha = \frac{1}{W_n - W_{n'}} \sum_{mm'} \left(T_{n'}^{m'}\right)^\dagger T_n^m \frac{\partial H_{m'm}}{\partial \alpha}. \tag{9}$$

All the components of the NACME are arranged in a vector denoted by $\mathbf{d}_{n'n}$.

The calculation of the NACME using Eq. (9) is analogous to that given previously by Preston and Tully[44] and applied to the DIM Hamiltonian of the H_3^+. Below, we shall apply it to the TRIM+MB Hamiltonian for H_4^+ and H_5^+.

Reuse of AIP Publishing content is subject to the terms: https://publishing.aip.org/authors/rights-and-permissions. Downloaded to IP: 161.111.22.69 On: Thu, 04 Aug 2016 09:50:28

B. TRIM+MB method for H_n^+

In this work, we use the DIM and/or TRIM representation, improved by including many-body interactions, generally called TRIM+MB, described in detail previously.[21,22]

The basis set used is an antisymmetrized product of an orbital and a spin part, $\varphi_m = \mathcal{A}\phi_i S_I$, with $m \equiv iI$, corresponding to linear combinations of Slater determinants or configurations, $\mathcal{A}$ being the anti-symmetrization operator. When applied to H_n^+, we use for the orbital part the minimum basis set of 1s orbitals in each hydrogen atom, which for the H_4^+ case is written as

$$\phi_i = s_j(1)\, s_k(2)\, s_l(3) \tag{10}$$

corresponding to an electron hole on nuclei i, and one electron in each $1s$ function of the rest of nuclei ($i,j,k,l = 1,2,\ldots$ cyclic and $j = i+1, k = j+1, l = k+1$).

We use a complete set of spin functions for 2–4 electrons to describe $H_3^+(1^1A', 1^3A')$, $H_4^+(^2A)$, and $H_5^+(^1A)$. For H_3^+ either one singlet or one triplet function is needed. However, for $H_4^+(^2A)$ and $H_5^+(^1A)$, two spin functions are needed to describe the doublet and singlet states, respectively. Thus, the total basis is composed by 3, 8, and 10 functions for H_3^+, H_4^+, and H_5^+, respectively.

The electronic Hamiltonian matrix is partitioned as

$$H = H^{TRIM} + H^{MB}, \tag{11}$$

where H^{TRIM} is the TRIM electronic matrix (DIM matrix for H_3^+), and H^{MB} is the many-body term matrix added to get the desired accuracy.

H^{MB} matrix elements are constructed[45,46] as permutationally invariant linear combinations of products of Rydberg polynomials, depending on the internuclear distances R_{ij} between atoms i and j. The parameters of these polynomials are fitted to minimize the difference between the energies obtained in this representation and *ab initio* points calculated at the higher accuracy. In the present implementation, H^{MB} is a diagonal matrix in which all H_{mm} terms are equal, corresponding to many-body terms added to reproduce the ground state of each of the systems considered.

The H^{TRIM} is the total electronic Hamiltonian rewritten as a sum of in triatomic and diatomic fragment terms and is formally exact. In the case of H_4^+ for the electronic configuration corresponding to an electron hole at nuclei i, it can be written as[21]

$$H_i^{TRIM} = \sum_{n>i,o>n} \hat{H}^+_{ino}(n-i,o-i) - \sum_{p>i} \hat{H}^+_{ip}(p-i) \tag{12}$$

(please note in Eq. (4) of Ref. 21 that the sign of the monoelectronic $\hat{H}^+_{ip}(p-i)$ Hamiltonians, the second term in the rhs, is wrong and should be negative). For H_5^+, it is written as[22]

$$H_i^{TRIM} = \sum_{n>i,o>n} \hat{H}^+_{ino}(n-i,o-i) - 2\sum_{p>i} \hat{H}^+_{ip}(p-i). \tag{13}$$

In these expressions, $H^+_{ip}(p-i)$ are monoelectronic Hamiltonians of H_2^+ fragments and $H^+_{ino}(n-i,o-i)$ are bielectronic Hamiltonians (for electrons $n-i, o-i$) describing H_3^+ for the *ino* nuclei. The i,n,o,p indexes are defined in a cyclic way and runs up to 4 and 5, for H_4^+ and H_5^+, respectively.

The evaluation of the matrix elements of $\hat{H}^+_{ip}(p-i)$ describing H_2^+ is simple, since they can be directly deduced from *ab initio* points obtained for few electronic states, the ground state on each symmetry box (see the Appendix of Ref. 22). The usual method is to fit these points to analytical functions, allowing a simple way to evaluate the derivatives as a function of internuclear distances. This is the same as it is usually done in the DIM approach.

The matrix elements of the triatomic Hamiltonians,

$$\left\langle \phi_j \left| \hat{H}^+_{ino}(n-i,o-i) \right| \phi_i \right\rangle, \tag{14}$$

correspond to diagonal and non-diagonal matrix elements involving linear combination of spin adapted diabatic matrices of H_3^+, of the first three electronic states of singlet and triplet symmetry. A good description of these triatomic matrix elements is what allows an accurate description of H_4^+ and H_5^+ systems, specially at long distances needed to properly describe collisions at low energies. For the evaluation of the matrix elements of the triatomic Hamiltonian, we use a generalization of DIM+MB method,[17] which is formally analogue to the TRIM and which is briefly described below.

C. DIM+MB method for H_3^+

The electronic Hamiltonian in the DIM approach[13–16] is expressed as a sum of atomic and diatomic fragment terms, and for H_3^+, it is written as[22]

$$H_i^{DIM} = \sum_{n>i,o>n} \hat{H}_{no}(n-i,o-i) + \sum_{p>i} \hat{H}^+_{ip}(p-i), \tag{15}$$

where $\hat{H}_{no}(n-i,o-i)$ are the bielectronic Hamiltonians of H_2. This Hamiltonian is formally exact. The approximation is in the use of a small basis set that introduces inaccuracies. To improve the accuracy, 3-body terms are added, $H^{MB} \equiv H^{3B}$, as indicated in Eq. (11). Thus, the triatomic electronic Hamiltonians involved in Eqs. (12) and (13) can be rewritten as

$$\hat{H}^+_{ino}(n-i,o-i) = H_i^{DIM}(n-i,o-i) + H^{3B}. \tag{16}$$

The triatomic DIM 3×3 matrices of H_3^+ are given by Ref. 17 for the singlet and by Ref. 47 for the triplet state. The H^{3B} here is also considered as a diagonal matrix, whose elements are all equal, as described above.

In the H^{3B}, the long range interactions are included, describing the interaction of the H^+ with the induced electric dipole and quadrupole of H_2,

$$V_{H_2\cdots H^+}(\mathbf{R},\mathbf{r}) = Q_2(r)P_2(\cos\theta)R^{-3} - \left[\frac{1}{2}\alpha_0 + \frac{1}{3}\left(\alpha_\parallel - \alpha_\perp\right)P_2(\cos\theta)\right]R^{-4}, \tag{17}$$

where $\alpha_0, \alpha_\parallel, \alpha_\perp$ are the average, parallel, and perpendicular polarizabilities and depend on the internuclear distance r and $\cos\theta = \mathbf{R}\cdot\mathbf{r}/rR$. The interaction of H_2^+ with H is considered as two $H^+ - H$ interactions,

$$V_{H^+\cdots H}(R) = -\frac{9}{4}R^{-4} - \frac{15}{2}R^{-6}, \tag{18}$$

which are already included in the mono-electronic terms that correspond to H_2^+ fragments, $H^+_{ip}(p-i)$.[19] Being included in

Reuse of AIP Publishing content is subject to the terms: https://publishing.aip.org/authors/rights-and-permissions. Downloaded to IP: 161.111.22.69 On: Thu, 04 Aug 2016 09:50:28

the diatomic terms, the $H_2^+ + H$ long range terms are included in all the $H^+ + H_2$ asymptotes, while it should not and has to be subtracted properly. Moreover, there are three equivalent rearrangement channels all tending to the same long range interactions so that it cannot be repeated either.

Let us consider a triangular configuration characterized by the internuclear distances $R_i = P_{i+2} - P_{i+1}$ (i = 1, 2, 3 cyclic), where the charge is in atom i and P_{i+1} is the position vector of atom $i+1$. The weighting function $w_i = \frac{e^{-2R_i^2}}{\sum_j e^{-2R_j^2}}$ is defined to include the LR interaction as

$$V_i^{LR}(R_i, R_{i+1}, R_{i+2}) = w_i \left\{ V^{H_2\cdots H^+}(\mathbf{R}, \mathbf{R}_i) - V_{H^+\cdots H}(R_{i+1}) - V_{H^+\cdots H}(R_{i+2}) \right\}, \quad (19)$$

where the $\mathbf{R} = [\mathbf{R}_{i+1} + \mathbf{R}_{i+2}]/2$ is the corresponding Jacobi vector. This form is slightly different to that used previously in Ref. 19 and has the advantage that its derivatives are continuous. Also, the Jacobi vector $\mathbf{R}$ can only reach the value of zero when the corresponding internuclear R_i distance is very long, and in this situation, the weight W_i becomes zero, i.e., this function acts as a damping function.

Including the long range term as a contribution in the H^{3B} allows to describe very accurately the long range behavior in H_3^+. In addition, in the TRIM+MB method, several triatomic fragments are considered, and these long range terms are involved in each of them, thus allowing to describe the delocalization of the charge in H_2^+ or H_3^+ when accounting for the $H_2^+ + H_2$ or $H_3^+ + H_2$ long range interactions.

For example, in Fig. 1, we show the long range dependence of the $H_2 + H_2^+$ interaction potential, for distances $R > 10$ a.u. For $R > 20$ a.u., the TRIM+MB potential fits very well the long range potential of Eq. (17). However, for $10 < R < 20$ a.u., the potential is better fitted using $C/R^{4.16}$. This is due to the contribution of two triatomic terms, each one with a charge in one of the two atoms of H_2^+. At these intermediate distances, the potential does not yet reach its long range behavior, what has some influence in the collision dynamics, as described below.

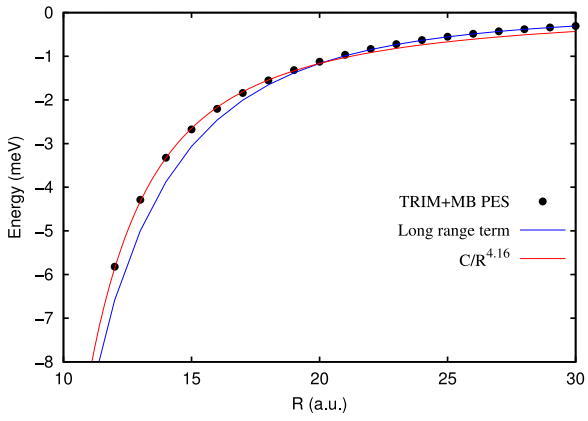

FIG. 1. Interaction potential for the H_2 ($r_1 = 1.4$ a.u.) + H_2^+ ($r_2 = 2$ a.u.) interaction as a function of the distance R between their centers of mass. The two molecules are in the plane, with $\mathbf{r}_1$ and $\mathbf{r}_2$ being parallel and perpendicular to $\mathbf{R}$. The internuclear distances r_1 and r_2 approximately correspond to their equilibrium distances.

The error of the potential in $10 < R < 20$ a.u. region is of the order of 1 cm^{-1}, when compared with the *ab initio* points. In some configurations, the *ab initio* points are better fitted by Eq. (17). Thus, we conclude that some more work has to be done to check the influence on the dynamics described below. Some work in this direction is currently under way.

The derivative of all the $\hat{H}^+_{ino}(n-i, o-i)$ and $\hat{H}^+_{ip}(p-i)$ can be evaluated analytically, and hence those of the full diabatic matrices, $\frac{\partial H_{m'm}}{\partial \alpha}$, required in Eqs. (8) and (9). These analytical derivatives were implemented to evaluate the derivative of the potential of the ground states of H_n^+ and compared with the numerical ones, giving excellent results. In addition, they were used in classical trajectory calculations, giving lower errors in conserving the total energy than the numerical ones.[25]

The minimum energy paths (MEPs) of the first states of H_3^+, H_4^+, and H_5^+ are shown in Fig. 2. For H_3^+ and H_4^+, the ground state potential crosses with the first excited state at intermediate distances, due to the charge transfer between the fragments. The three codes, for n = 3–5, are available upon request.

D. MDQT

The non-adiabatic dynamics is studied in the adiabatic representation with the MDQT method as developed and described by Tully.[29] Here, only some details on the numerical implementation made in this work are described.

An electronic wave-packet is expanded as $\Psi(\mathbf{R}[t]) = \sum_n^{n_{max}} c_n(t)\phi_{n'}$, with $c_n(t=0) = \delta_{in}$ determining the initial conditions. Its evolution in time is governed by[29]

$$i\hbar\dot{c}_n(t) = \sum_l \left[W_l \delta_{nl} - ih\dot{\mathbf{R}} \cdot \dot{\mathbf{d}}_{kl} \right] c_l(t). \quad (20)$$

These coupled equations are integrated in time using a split operator propagator,[48] along a classical trajectory $\mathbf{R}(t)$. To avoid numerical problems at conical intersections, where the non-adiabatic couplings diverge, the NACMEs are truncated so that $-ih\dot{\mathbf{R}} \cdot \dot{\mathbf{d}}_{kl} \leq E_{max}$. In these expressions, $\dot{\mathbf{R}}$ is the multidimensional velocity vector, corresponding to the $3 \times N$

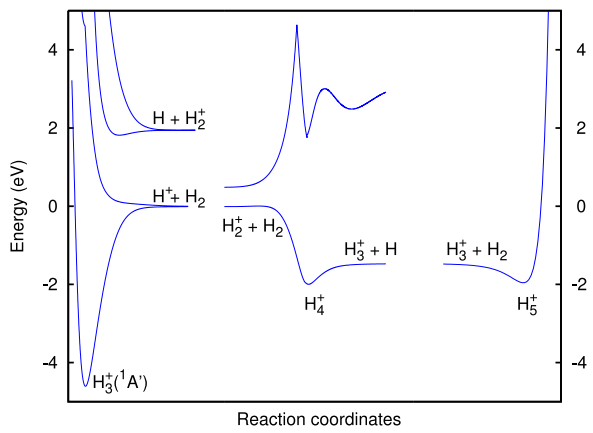

FIG. 2. Minimum energy paths (in eV) of the lowest electronic states of H_3^+, H_4^+, and H_5^+. In each system, a different zero of energy is chosen to plot all of them together.

Reuse of AIP Publishing content is subject to the terms: https://publishing.aip.org/authors/rights-and-permissions. Downloaded to IP: 161.111.22.69 On: Thu, 04 Aug 2016 09:50:28

Cartesian coordinates of the position vectors of the N atoms.

The classical trajectories $\mathbf{R}(t)$ are obtained solving the Hamilton equations of motion in the $6N$ generalized coordinates using a step adaptive Adams-Bashforth-Moulton predictor-corrector method.[49] At each time step, the switching probability, g_{if}, from electronic state i to each f is calculated as[29]

$$g_{i,f} = \frac{\Delta t}{|c_i|^2}\left[2Re(c_i c_f^* \dot{\mathbf{R}} \cdot \dot{\mathbf{d}}_{if})\right], \tag{21}$$

so that the sum of all these probabilities is 1. These probabilities are then considered consecutively in a vector as $G_i = g_{i,i+1}, G_{i+1} = G_i + g_{i,i+2}, \ldots$. Then, a random number, ξ, is selected and if it lies in the $G_f < \xi < G_{f+1}$, a switch to state f is done if the energy condition,

$$E_i^{kin}(\dot{\mathbf{R}}) + W_i(\mathbf{R}) = E_f^{kin}(\dot{\mathbf{R}}') + W_f(\mathbf{R}), \tag{22}$$

is fulfilled. To accomplish this, the velocities, $\dot{\mathbf{R}}$, in the new f state are changed along the $\mathbf{d}_{if}$ vector as

$$\dot{\mathbf{R}} \rightarrow \dot{\mathbf{R}}' = \dot{\mathbf{R}} + \beta \mathbf{d}_{if}, \tag{23}$$

where β is chosen to accomplish Eq. (22). If this condition is not possible, with an error lower than $\epsilon = 10^{-12}$ a.u., the switch is not done and the trajectory is continued in the same i electronic state.

In order to get the reaction cross section for the reaction

$$H_2^+(v, j = 0) + H_2(v' = 0) \rightarrow H_3^+ + H, \tag{24}$$

a Monte Carlo sampling of initial conditions is performed. The method used is completely analogous to that introduced by Karplus *et al.*[50] In order to distinguish between H_2 and H_2^+ in a single electronic state, we take the inner classical turning point for H_2 and the outer turning point for H_2^+ in their respective initial vibrational states, for a reason which will become clear below. More than 10^5 trajectories are run for each energy and initial state. The energy conservation in all of them is better than 0.001 cm^{-1}.

In order to get an approximate relationship between the non-adiabatic transitions and the non-adiabatic matrix elements, we shall use the inverse of the Massey parameter[38,44] defined as

$$M_{if}^{-1} = \frac{\dot{\mathbf{R}} \cdot \dot{\mathbf{d}}_{if}}{2(W_i - W_f)}. \tag{25}$$

III. APPLICATION TO H_4^+

A. Non-adiabatic couplings

As shown in Fig. 2, the first two electronic states are separated by ≈0.5 eV in the $H_2 + H_2^+$ entrance channel, which is close to the sum of the vibrational zero-point energies of the reactants. These two states cross at configurations where the two diatomic molecules have the same internuclear distances, as can be seen in the top panel of Fig. 3. In a pure adiabatic representation, the positive charge is not located in any of the two diatomic fragments, but it is delocalized. When the two internuclear distances are the same, the charge has an equal probability of being in either one of the two first lower electronic states giving rise to two degenerate states, i.e., to a crossing.

In the middle panels of Fig. 3, some cuts of the potential energy for the first two adiabatic states are shown as a function of the internuclear distance r_1 of the first diatomic fragment. The other diatom is frozen for three values, r_2 = 1.4, 1.7, and 2 a.u. All the other coordinates are frozen, with the two bonds parallel in a plane. Three different energies are plotted: the *ab initio* points (calculated at Multi-Reference Configuration Interaction (MRCI) level using the MOLPRO package[51] as described in Ref. 21), results obtained with the TRIM+MB (labeled TRIM) described here, and finally the energies obtained with the DIM approach. The DIM energies are rather good in the $H_2^+ + H_2$ entrance channel but already show some disagreements with the *ab initio* ones. The TRIM+MB results for the ground state are excellent, since the MB term is adjusted for that, showing some discrepancies for the excited electronic state. Nevertheless, for the collision energies of interest, below 1 eV, these results are considered to be accurate enough, giving a rather good description of the crossings.

The NACMEs obtained with these three methods are shown in the bottom panels of Fig. 3. Note that the TRIM+MB method gives DIM results when removing the MB terms in the triatomic fragments and in the H_4^+ potential. The *ab initio* results are obtained with the MOLPRO package, using a first order difference method with an interval of 0.01 a.u. For the square geometry, r_2 = 2 a.u., the crossings and the NACME obtained with the three methods are in very good agreement. As r_2 distance decreases, TRIM and DIM results remain very close but their differences with respect to the *ab initio* results increase. These differences are considered to be rather small and are neglected here.

The TRIM NACMEs are only slightly better as compared to the DIM results. The reason is that the adiabatic wave-functions are obtained from the approximated H^{TRIM} Hamiltonian, in whose triatomic terms and the diagonal H^{3B} term are all the same. Under this condition, the DIM and TRIM NACMEs are very similar. The inclusion of the "exact" H^{3B} terms in the H^{TRIM} method would improve the description of the crossings and the accuracy of the NACME. Work in this direction is in progress.

Summarising, the TRIM+MB improves significantly the accuracy of the ground adiabatic state, including the long-range interactions and triatomic fragments, as described previously.[21] In addition, it improves the position of the curve crossing in the entrance channel with respect to the DIM approach. The NACMEs of the TRIM method with the approximations made so far are very similar to those obtained with the DIM approach, and both are pretty similar to the *ab initio* results.

These results are analogous to all the geometries and distances analyzed in the entrance channel. In the $H + H_3^+$ products channels, the ground and excited states separate, and non-adiabatic effects become negligible. We therefore conclude that the present approach is a significant improvement with respect to the previous DIM method used to study the non-adiabatic dynamics in this system.

Reuse of AIP Publishing content is subject to the terms: https://publishing.aip.org/authors/rights-and-permissions. Downloaded to IP: 161.111.22.69 On: Thu, 04 Aug 2016 09:50:28

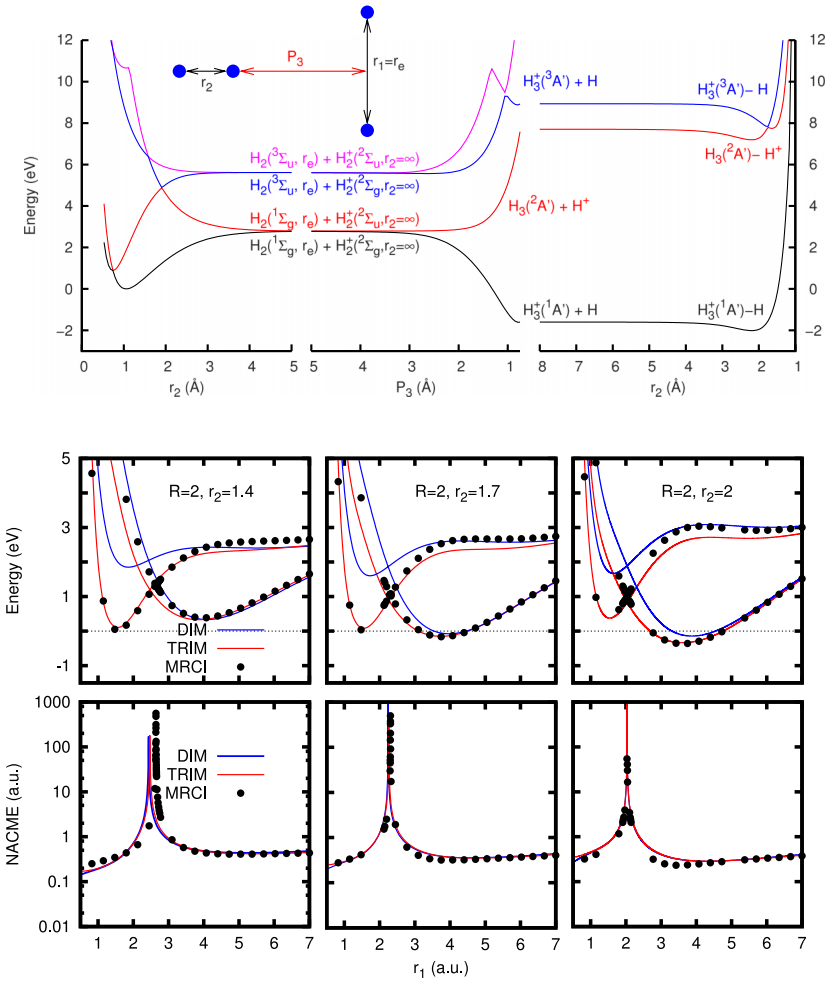

FIG. 3. Top panel: Energy diagram of the lowest electronic states of H_4^+ showing curve crossings as a result of charge transfers between equivalent subunits. Middle panels show the potential energy curves and bottom panels the NACME, obtained for two parallel H_2 fragments in a plane at fixed values of $R = 2$ a.u. (the distance between the two centers of mass) and $r_2 = 2$ a.u. and by varying the internuclear distance of the first H_2 subunit, r_1. The NACME is calculated in Cartesian coordinates, and here, only one is shown, along the z component of r_1. The DIM, TRIM, and MRCI label the method used to obtain the energies or NACMEs.

B. Reactive collision cross sections

This reaction has 10 rearrangement channels

$$
\begin{aligned}
AB^+ + CD &\longrightarrow AB^+ + CD && \text{inelastic}\\
&\longrightarrow AB + CD^+ && \text{electron transfer}\\
&\longrightarrow \begin{Bmatrix} A + BCD^+ \\ B + ACD^+ \end{Bmatrix} && \text{proton hop}\\
&\longrightarrow \begin{Bmatrix} ABC^+ + D \\ ABD^+ + C \end{Bmatrix} && \text{atom hop}\\
&\longrightarrow \begin{Bmatrix} AC^+ + BD \\ AC + BD^+ \\ AD^+ + BC \\ AD + BC^+ \end{Bmatrix} && \text{exchange.}
\end{aligned}
\tag{26}
$$

The electron transfer channel is included within the first adiabatic electronic state, as discussed later, in which the charge is in either of the two fragments and can only be distinguished in the dynamical calculations by the vibrational frequency when the distance between the two diatomic fragments is long.

Proton hop and atom hop mechanisms both yield to H_3^+ products and have relatively similar cross sections, as shown in Fig. 4. The proton hop mechanism has a slightly higher cross section, probably because the H_2^+ fragment with a larger equilibrium distance is easier to brake.

The exchange mechanism is about 100 times lower. This mechanism involves two atoms or proton hops or a simultaneous exchange. This reaction is rather direct, and the reaction occurs without giving time to a second atom/proton transfer. This could explain why the exchange mechanisms present lower cross sections.

The proton and atom hop mechanisms cannot be separated, and only two products can be distinguished, $H_2^+ + H_2$ and $H_3^+ + H$, because all the hydrogen atoms are

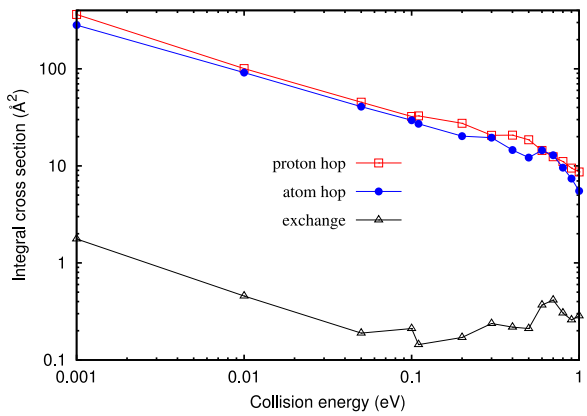

FIG. 4. Cross sections (in Å^2) for the $H_2(v' = 0, j' = 0) + H_2^+(v = 0, j = 0)$ collisions for the different arrangement channels indicated in Eq. (26) as calculated here with the MDQT method.

Reuse of AIP Publishing content is subject to the terms: https://publishing.aip.org/authors/rights-and-permissions. Downloaded to IP: 161.111.22.69 On: Thu, 04 Aug 2016 09:50:28

indistinguishable. This is a fundamental principle of quantum mechanics, and in order to distinguish among some channels, it is necessary to substitute one or several hydrogen atoms by an isotope.

In this work, we present MDQT calculations for the $H_2(v'=0,j'=0)+H_2^+(v,j=0)$ collisions, always keeping the reactants in their ground rovibrational state, except in Section III C, where the effect of the initial vibrational excitation of $H_2^+(v)$ is analyzed. Unless otherwise indicated, the first two adiabatic electronic states have been included.

In Fig. 5, we compare the total reaction probability, the sum of proton hop and atom hop, with previous experimental[35,52] and theoretical results.[36,53] In all cases, the agreement is very good. The merged beam results of Glenewinkel-Meyer and Gerlich[35] were obtained with H_2^+ ions produced in a storage ion source. The relative error is due to the calibration of the target density and, therefore, constant over the energy range shown. Thus, our MDQT results are all within the experimental error bars.

The previous results of Eaker and Schatz[36] for collision energies higher than 0.3 eV are also in good agreement with the results presented here. Those results were obtained using the DIM potential of Stine and Muckerman,[38] using also a variation of a surface hopping method. This indicates that at this intermediate energies, the DIM approach is rather good in describing the total reaction cross section. The quantum mechanical results of Baer and Ng[53] are lower than the present results, and this may be explained by their use of a lower dimensional model needed to perform their calculations.

The Langevin model gives results significantly lower than the results obtained here, what means that the interaction potential averaged over the $H_2(j'=0)$ rotation does not vary as $-\alpha/2R^4$. At the collision energies of 1, 10, and 50 meV, the maximum impact parameter for the reaction is found to be 30, 15, and 10 a.u., respectively. As discussed above, for these "intermediate" distances, the averaged potential does not follow the C/R^4 long range behaviour but it is better fitted by adding a $-C/R^{4.16}$ term (see Fig. 1). In this reaction, once the $H_3^+ + H$ product channels are reached, there is no return back to the entrance channel, and the capture models are then applicable here. According to these models, the cross section takes the form[54]

$$\sigma(E) = \pi\, q(s)\,(C/E)^{2/s} \quad \text{with} \quad q(s) = \frac{s/2}{[(s-2)/2]^{(s-2)/s}}. \tag{27}$$

The MDQT cross section of Fig. 5 is perfectly fitted by this expression for E < 0.1 eV, with $C = 11.51$ Å^s eV and $s = 4.16$. This value of s is in agreement with the dependence of the potential in the region $10 < R < 20$ a.u. To get the Langevin results, much lower collision energies have to be considered, involving longer distances, at which the average interaction potential varies as $\propto R^{-4}$. This can be explained knowing that in this system, the positive charge is not punctual, but it is distributed in H_2^+.

For collisions of H_2 with atomic cations, it is expected that at these energies of 1-100 meV, the asymptotic Langevin limit is already achieved, since the charge can be considered punctual. This is, for example, the case of $H_2 + O^+$ in experimental[55] as well as in theoretical simulations.[56] However, to check this finding in $H_2 + H_2^+$ collisions, a better fit of the $10 < R < 20$ a.u. region, with much lower errors, should be obtained.

C. Effect of initial vibrational excitation

The possibility of generating H_2^+ in different vibrational states made possible many experimental and theoretical studies for its effect.[32,34–37] Here, we analyze the effect of $H_2^+(v = 0,1,2,3)$ initial vibrational states in the formation of H_3^+ in the 0-1 eV translational energy range, as shown in Fig. 6. The behaviour of all of them is very similar, being nearly parallel as a function of energy, clearly demonstrating that the capture model is valid in all the cases.

The small decrease of the cross section of the H_3^+ formation as v increases is not explained by the increase of the exchange cross section, in the right panel of Fig. 6. When the two mechanisms are added, the resulting plot is very close to that shown in the left panel. This exchange

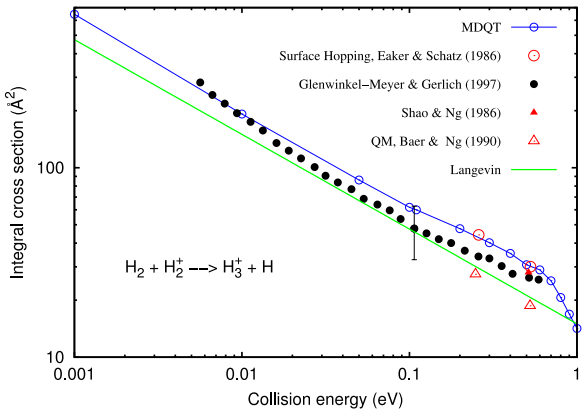

FIG. 5. $H_2(v'=0,j'=0)+H_2^+(v=0,j=0)\rightarrow H_3^+ + H$ total reaction cross sections (in Å^2) obtained with the MDQT method, compared with the experimental data of Glenewinkel-Meyer and Gerlich[35] and Shao and Ng,[52] and with theoretical simulations, the QCT results of Eaker and Schatz[36] and the 3 dimension quantum mechanical results of Baer and Ng.[53]

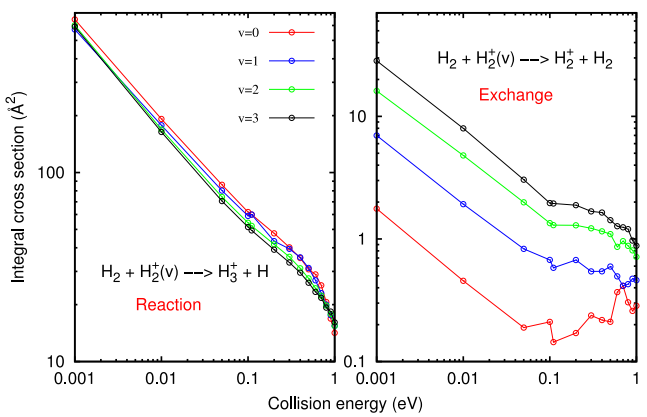

FIG. 6. Left panel: $H_2+H_2^+(v=0,1,2,3)\rightarrow H_3^+ + H$ and right panel: $H_2 + H_2^+(v=0,1,2,3)\rightarrow H_2^+ + H_2$ exchange cross sections (in Å^2), obtained with the MDQT method considering 2 adiabatic electronic states. The two reagents are initially in their ground rotational state.

Reuse of AIP Publishing content is subject to the terms: https://publishing.aip.org/authors/rights-and-permissions. Downloaded to IP: 161.111.22.69 On: Thu, 04 Aug 2016 09:50:28

TABLE I. Experimental[32] and simulated cross sections (Å^2) for the $H_2(v'=0, j'=0) + H_2^+(v, j=0) \rightarrow H_3^+ + H$ reaction as a function of the vibrational excitation of H_2^+ for 0.1 eV of translational energy.

v	Experiment[32]	Simulated
0	51 ± 2	59.9
1	45 ± 3	59.9
2	46 ± 3	52.2
3	42 ± 3	49.4

mechanism has a much lower cross section, but its increase with v is rather important.

The experimental measurements indicate this trend for the formation of H_3^+, as listed in Table I. The absolute value 51 ± 2 Å^2 of the cross section of Koyano and Tanaka[32] is lower at 0.1 eV than the present result of 59.9 Å^2. The experimental results of Glenewinkel-Meyer and Gerlich[35] in Fig. 5 is also lower, being 48 ± 13 Å^2 at 1.0 eV. The systematic deviation of the cross sections on the collision energy may be due to rovibrational excitation of the ions. However, the error bars in these last experiments were estimated to be larger, of the order of 15 Å^2, and the simulated values lie within these larger error bars. For this reason, we consider the present values rather good in describing the reaction cross section, noting that there is a qualitative agreement of the trends with increasing v between the experimental and theoretical values. In addition, the adequacy of the classical method used here should be tested by doing quantum dynamical simulations.

What is the origin of the decrease of the H_3^+ formation cross section as vibrational excitation increases? One possibility is the non-adiabaticity due to the curve crossing with the first excited state, as shown in Fig. 3. To check this, we have performed the same calculations but including only the ground electronic state, i.e., pure QCT calculation, shown in Fig. 7. The QCT cross section shows a similar trend as compared to those shown in Fig. 6 obtained with 2 electronic states. However, the H_3^+ formation cross sections for different v's are closer and with a different ordering. This may be taken as an indication that the small differences observed in the left panel of Fig. 6 are due to non-adiabatic effects.

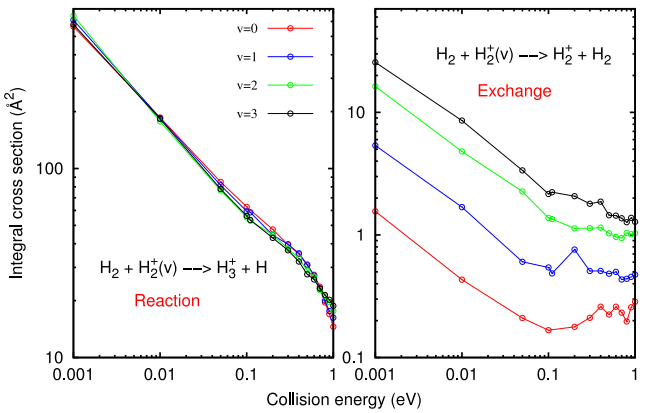

FIG. 7. Same as Fig. 6 but considering only the ground electronic state, thus being denoted as QCT results.

The MDQT and QCT exchange cross sections shown in the right panels of Figs. 6 and 7 are very similar for collision energies below 0.1 eV. However, for larger energies, the oscillations differ considerably, and these differences are attributed to non-adiabatic effects.

Experimentally, there are no results studying the effect of the neutral $H_2(v')$ vibrational excitation. However, since the variations are due to non-adiabatic effects (as discussed in more detailed below), we do expect a similar qualitative behaviour when exciting either of the two diatomic reagents, H_2^+ described above or H_2.

D. Non-adiabatic dynamics

The lowest two adiabatic states of H_4^+ cross at relatively low energies in the $H_2 + H_2^+$ entrance channel and then separate in the $H_3^+ + H$ products channel, as can be seen in the middle panel of Fig. 2. The origin of this crossing is that at asymptotic distances, there are two equivalent diabatic states, $H_2 + H_2^+$ and $H_2^+ + H_2$, which combine to form the adiabatic state in which the charge is delocalized between the two fragments. This situation is similar to that of H_2^+, in which two diabatic states are obtained, of gerade and ungerade symmetries.

In the ground adiabatic state of H_4^+, at long distances between H_2 and H_2^+ center of masses, R, when one of the diatomic fragments is frozen at the H_2 equilibrium distance, the other fragment presents a potential diabatic curve similar to H_2^+, and vice versa. However, the adiabatic states present crossings with cusps as represented in Fig. 8. If the two fragments are kept in their ground vibrational state, the two H_2 and H_2^+ internuclear distances never get the same value at the asymptote simply because their turning points are slightly separated. This is a classical effect, since the quantum wave-functions penetrate in the potential and overlap.

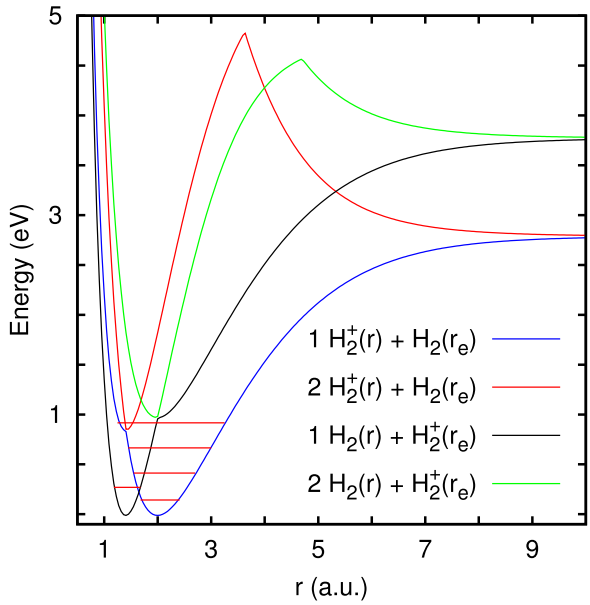

FIG. 8. Potential energy cuts obtained by freezing r_{34} internuclear distance to the equilibrium value of H_2^+ ($r_2 \approx 2$ a.u.) and r_{12} to the equilibrium value of H_2 ($r_1 \approx 1.4$ a.u.) and varying the other.

Reuse of AIP Publishing content is subject to the terms: https://publishing.aip.org/authors/rights-and-permissions. Downloaded to IP: 161.111.22.69 On: Thu, 04 Aug 2016 09:50:28

When H_2^+ gets vibrationally excited, its inner classical turning point is shorter than the outer one of H_2, see Fig. 8. In this situation, even at long distances among the diatoms, R, the diatomic internuclear distances, r_1 and r_2, can get the same value. At this configuration, there is a crossing at which the non-adiabatic couplings, shown in Fig. 3, are large and may induce non-adiabatic transitions. As the vibrational excitation increases, the possibility that $r_1 = r_2$ increases and therefore the probability of electronic transitions.

All these are illustrated in Figs. 9 and 10, in which we show several quantities associated to two trajectories leading to H_3^+ products, one starting in $H_2^+(v = 0)$ and the other in $H_2^+(v = 2)$. The initial conditions for the two trajectories are very similar, except in the initial H_2^+ internuclear distance, r_2, corresponding to the outer turning points for $v = 0$ and 2, respectively. In Fig. 9, the two internuclear distances (in the second panel from the bottom) never cross for $R > 10$ a.u. (bottom panel), and as a consequence, there is no electronic transition. The quantum wave-packet (top panel) always

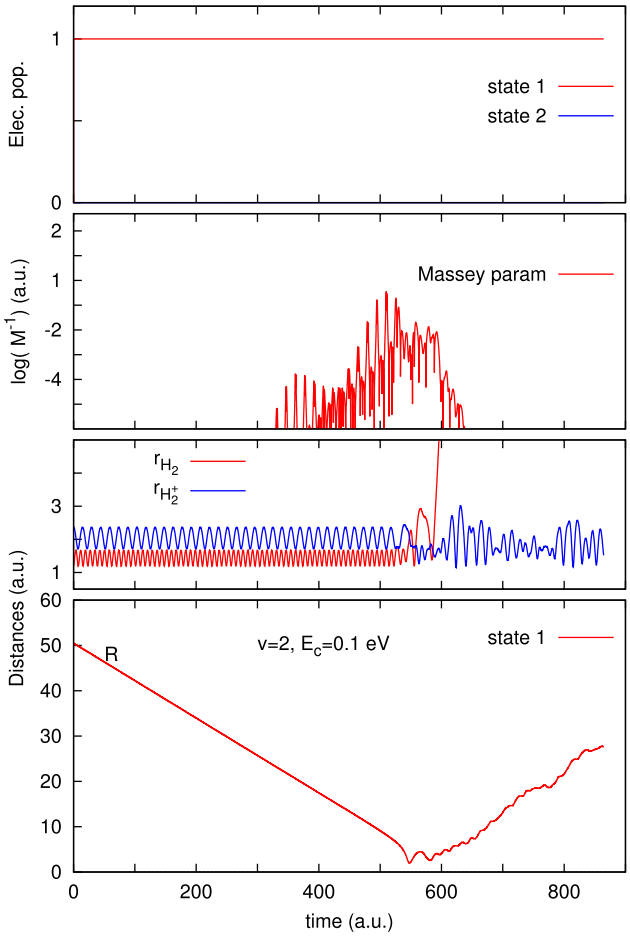

FIG. 9. MDQT trajectory for the $H_2 + H_2^+(v = 0) \rightarrow H_3^+ + H$ collision. Bottom panel indicates the distance R between the centers of mass of the two diatomic molecules (in red is in the ground electronic state and in blue is in the excited electronic state). Second panel from bottom shows the two internuclear distances, r_1 (red) and r_2 (blue), initially corresponding to H_2 and H_2^+. Third panel from bottom shows the inverse of the Massey parameter along the trajectory. Since there is only one NACME, M_{ij} has been replaced by M in the y label. Top panel shows the state population of the electronic wave-packet.

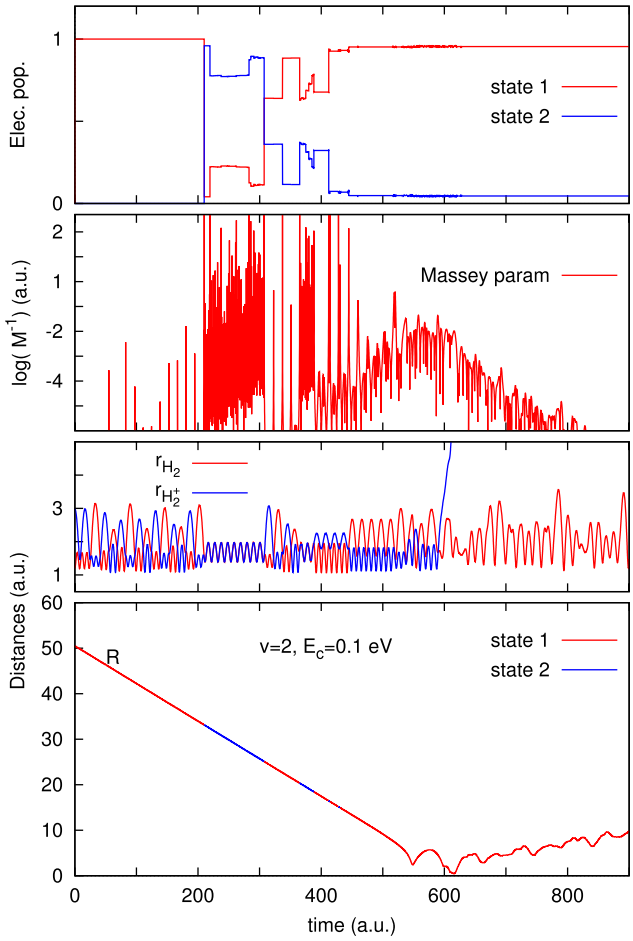

FIG. 10. Same as Fig. 9 but for the $H_2 + H_2^+(v = 2) \rightarrow H_3^+ + H$ collision.

remains in the ground electronic state, and the inverse Massey parameter, Eq. (25), only gets significant values for $R < 20$ a.u.

When starting in $H_2^+(v = 2)$, in Fig. 10, the situation changes dramatically. The amplitude of the H_2^+ vibration increases, and in this case, r_1 and r_2 may get the same value. For time <200 a.u., it can be seen that the red and blue curves exchange between them, i.e., an electron transfers between the two diatoms. This is already surprising since it happens at distances $R > 30$ a.u. and in one single adiabatic electronic state. Such exchange of charge occurs when $r_1 \approx r_2$.

When the distance R decreases, and $r_1 \approx r_2$, the non-adiabatic couplings become larger, as illustrated by the inverse Massey parameter in the third panel from bottom in Fig. 10. This makes that electronic transitions may take place even at relatively long distances, $R \approx 30$ a.u., promoting the system to the first excited electronic state. In this state, the motions of the two diatoms become in perfect phase, as shown in the second panel of Fig. 10 between $200 < time < 300$ a.u. This result is observed in all trajectories analyzed. The Massey parameter is always large, being able to induce a transition back to the ground state.

In reactive trajectories leading to H_3^+, the energy difference between the two electronic states in the products channel gets apart and the non-adiabatic couplings decrease. Thus, for these trajectories, the electronic transitions do not occur once the H_3^+ is formed. The four $H_3^+ + H$ product channels are separated

Reuse of AIP Publishing content is subject to the terms: https://publishing.aip.org/authors/rights-and-permissions. Downloaded to IP: 161.111.22.69 On: Thu, 04 Aug 2016 09:50:28

by a barrier of ≈0.25 eV which hinders the exchange among them in low temperature $H_3^+ + H$ collisions.[57,58]

For those trajectories leading to diatomic fragments, either in the inelastic or the exchange channels, the two electronic states remain close and the coupling is large. Therefore, the maximum number of transitions happens for these kind of trajectories.

The behavior of the two trajectories shown in Figs. 9 and 10, with similar initial conditions, is quite analogous, both leading to the same H_3^+ product. A careful analysis of many other trajectories leads us to conclude that the trajectories do not vary very much due to electronic transitions, and this is the reason why the reaction cross section does not vary significantly. The most affected trajectories are those leading back to any $H_2^+ + H_2$ channel, and this explains why vibrational excitation affects more significantly this channel.

Once the H_2^+ is vibrationally excited, the number of electronic transitions increases with decreasing collision energy, simply because it takes longer time for the two fragments to approach and therefore, $r_1 = r_2$ occurs many times. For $v = 0$, there are no electronic transitions even at $E = 1$ eV, with energy enough to allow transitions to excited electronic states. Thus, the collision dynamics of $H_2(v = 0) + H_2^+(v = 0)$ can be studied on a single electronic state.

E. Isotopic effect

H_3^+ is the universal protonator in cold molecular clouds. It is also responsible for the high deuterium fractionation of many hydrides in space, much higher than the natural abundance of the D with respect to H. It is therefore important to analyze how the reaction changes whenever one deuterium substitutes one hydrogen atom in either H_2 or H_2^+ reactants. Here, we present results for the H_2D^+ system, where the D is initially either in the ion or the neutral. As demonstrated above, considering the ground rovibrational state of the two reagents, the dynamics proceeds in a single adiabatic surface, and the usual QCT approach is used.

The total cross sections to form triatomic products, either H_3^+ or H_2D^+, are compared in Fig. 11. The cross sections for the three reactions considered are very similar, with the same dependence on energy, which can be explained by the capture model of Eq. (27).[54] There are only small differences at low and high energies.

In the two cases, there are three channels leading to H_2D^+ fragments and only one to H_3^+. Thus, assuming unbiased statistical scrambling, the cross section for the formation of the deuterated H_2D^+ is approximately 3 times that of H_3^+ in $H_2 + HD^+$ or $H_2^+ + HD$ collisions. The role of quantum effects, especially at low energies, may change this.

The differences arise when considering the possible mechanisms, i.e., the jump of neutral H or D or of a H^+ or a D^+, indicated in different channels of Eq. (26). These mechanisms are distinguished in Fig. 12 and are not equivalent when there is a deuterium. The channel which presents larger differences is that involving the hop of a deuterium, charged or neutral, for which at $E > 0.1$ eV is always smaller. This may be explained by an impulsive mechanism, in which heavier atoms are more difficult to deviate.

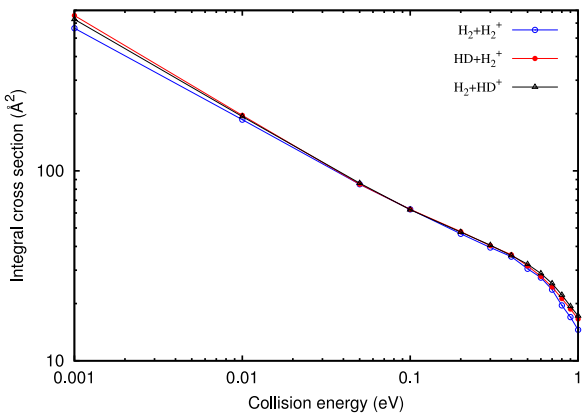

FIG. 11. Total reaction cross sections for the isotopic variants: $H_2 + H_2^+(v = 0)$, $HD + H_2^+(v = 0)$, and $H_2 + HD^+(v = 0)$ collisions.

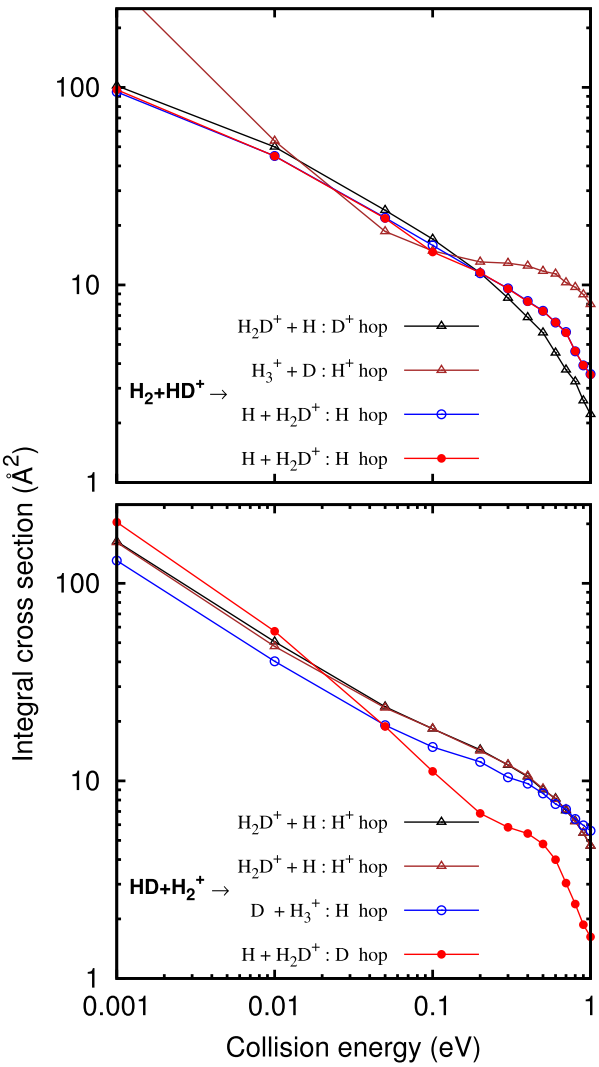

FIG. 12. Cross section for the 4 different rearrangement channels leading to triatomic products, in Eq. (26) for the $HD + H_2^+(v = 0)$ and $H_2 + HD^+(v = 0)$ collisions.

Reuse of AIP Publishing content is subject to the terms: https://publishing.aip.org/authors/rights-and-permissions. Downloaded to IP: 161.111.22.69 On: Thu, 04 Aug 2016 09:50:28

For low collision energies, however, the situation changes. In $HD + H_2^+$ collisions, the 4 channels present similar cross sections, while for $H_2 + HD^+$ collisions, the hop of a proton always prevails, probably because it combines the lower mass with the most elongated bond.

IV. CONCLUSIONS

In this work, we have developed analytical potential derivatives and non-adiabatic couplings for H_n^+ systems for TRIM+MB multi-state model potentials, allowing the accurate description of H_3^+ fragments and the inclusion of long range interactions. This procedure has been applied to the study of $H_2(v' = 0, j' = 0) + H_2^+(v, j = 0)$ reactive collisions, considering the effect of collision energy, vibrational excitation of H_2^+, and non-adiabatic and isotopic effects, using an implementation of the MDQT method of Tully.[29] The calculations have been restricted to the ground rotational levels and therefore do only explore the charge-induced dipole term of the long range interactions. The calculated cross sections are in good agreement with the available experimental data[35] and are slightly larger than those obtained with a Langevin model. The reason of that is that the effective average potential does not vary as R^{-4} for distances between 10 and 20 a.u., because the charge is distributed in the H_2^+ molecule and cannot to be centered at its center of mass.

There are small changes in the cross section when increasing the vibrational excitation of H_2^+ reactants, in agreement with the experimental data of Koyano and Tanaka,[32] which are attributed to non-adiabatic transitions to the first excited electronic state. These electronic transitions occur in the entrance channel when the two internuclear distances of the two diatomic species (H_2 and H_2^+) are equal, leading to a charge transfer between them, but with rather low cross sections at the energies studied here.

We conclude that for energies below 1 eV and starting in the ground vibrational states of reactants, the non-adiabatic effects are negligible. Then, pure QCT calculations are performed to study the isotopic effects in the $HD + H_2^+$ and $H_2 + HD^+$ collisions. Again, the cross sections are governed by the long range interactions. The different mechanisms (proton or atom hops, H or D) are distinguished and the D or D^+ hop mechanism is found to be the one with lower cross sections at $E > 0.1$ eV.

ACKNOWLEDGMENTS

F.N. acknowledges UOIT for the support of a sabbatical stay at IFF-CSIC, Spain. We acknowledge the support of Ministerio de Economía y Competitividad (Spain), for Grant Nos. CSD2009-00038 and FIS2014-52172-C2. The calculations have been performed in CESGA and CSIC computing centers, which are acknowledged. We also thank the support from the European Research Council under the European Union's Seventh Framework Programme (No. FP/2007-2013)/ERC Grant Agreement No. 610256 (NANOCOSMOS). We also acknowledge the COST Action No. CM1401 "Our Astrochemical History."

[1]E. Herbst and T. J. Millar, "The chemistry of cold interstellar cloud cores," in *Low Temperatures and Cold Molecules*, edited by I. W. M. Smith (Imperial College Press, London, 2008), p. 1.
[2]J. Tennyson, Rep. Prog. Phys. **58**, 412 (1995).
[3]E. Herbst, Philos. Trans. R. Soc., A **358**, 2523 (2000).
[4]T. Oka, Philos. Trans. R. Soc., A **370**, 4991 (2012).
[5]D. Gerlich, P. Jusko, Š. Roučka, I. Zymak, R. Plašil, and J. Glosík, Astrophys. J. **749**, 22 (2012).
[6]T. Oka, Chem. Rev. **113**, 8738 (2013).
[7]Special Issue on "Chemistry, Astronomy and Physics of H_3^+," edited by T. Oka, Philos. Trans. R. Soc., A **370**(1978) (2012).
[8]D. Gerlich, J. Chem. Phys. **92**, 1141 (1990).
[9]D. Gerlich and S. Schlemmer, Planet. Space Sci. **50**, 1287 (2002).
[10]T. J. Millar, A. Bernett, and E. Herbst, Astrophys. J. **340**, 906 (1989).
[11]L. Pagani, M. Salez, and P. G. Wannier, Astron. Astrophys. **258**, 479 (1992).
[12]B. J. McCall and T. Oka, Science **287**, 1941 (2000).
[13]F. O. Ellison, J. Am. Chem. Soc. **85**, 3540 (1963).
[14]F. O. Ellison, N. T. Huff, and J. C. Patel, J. Am. Chem. Soc. **85**, 3544 (1963).
[15]J. C. Tully, Adv. Chem. Phys. **42**, 63 (1980).
[16]P. J. Kuntz, "Interaction potentials. II. Semiempirical atom-molecule potentials for collision theory," in *Atom-Molecule Collision Theory: A Guide for Experimentalists*, edited by R. B. Bernstein (Plenum Press, New York, 1979), p. 79.
[17]A. Aguado, O. Roncero, C. Tablero, C. Sanz, and M. Paniagua, J. Chem. Phys. **112**, 1240 (2000).
[18]A. Aguado, M. Lara, M. Paniagua, and O. Roncero, J. Chem. Phys. **114**, 3440 (2001).
[19]L. Velilla, B. Lepetit, A. Aguado, J. A. Beswick, and M. Paniagua, J. Chem. Phys. **129**, 084307 (2008).
[20]L. P. Viegas, A. Alijah, and A. J. C. Varandas, J. Chem. Phys. **126**, 074309 (2007).
[21]C. Sanz-Sanz, O. Roncero, M. Paniagua, and A. Aguado, J. Chem. Phys. **139**, 184302 (2013).
[22]A. Aguado, P. Barragan, R. Prosmiti, G. Delgado-Barrio, P. Villarreal, and O. Roncero, J. Chem. Phys. **133**, 024306 (2010).
[23]T. González-Lezana, O. Roncero, P. Honvault, J. M. Launay, N. Bulut, F. J. Aoiz, and L. Bañares, J. Chem. Phys. **125**, 094314 (2006).
[24]E. Carmona-Novillo, T. González-Lezana, O. Roncero, P. Honvault, J. M. Launay, N. Bulut, F. J. Aoiz, L. Bañares, A. Trottier, and E. Wrede, J. Chem. Phys. **128**, 014304 (2008).
[25]S. Gómez-Carrasco, L. González-Sánchez, A. Aguado, A. Zanchet, and O. Roncero, J. Chem. Phys. **137**, 094303 (2012).
[26]K. Park and J. C. Light, J. Chem. Phys. **126**, 044305 (2007).
[27]E. Hugo, O. Asvany, and S. Schlemmer, J. Chem. Phys. **130**, 164302 (2009).
[28]K. N. Crabtree, C. A. Kauffman, B. A. Tom, E. Becka, B. A. McGuire, and B. J. McCall, J. Chem. Phys. **134**, 194311 (2011).
[29]J. C. Tully, J. Chem. Phys. **93**, 1061 (1990).
[30]J. R. Krenos, K. K. Lehmann, J. C. Tully, P. M. Hierl, and G. P. Smith, Chem. Phys. **16**, 109 (1976).
[31]G. Ochs and E. Teloy, J. Chem. Phys. **61**, 4930 (1974).
[32]I. Koyano and K. Tanaka, J. Chem. Phys. **72**, 4858 (1980).
[33]S. L. Anderson, F. A. Houle, D. Gerlich, and Y. T. Lee, J. Chem. Phys. **75**, 2153 (1981).
[34]J. E. Pollard, L. K. Johnson, D. A. Lichtin, and R. B. Cohen, J. Chem. Phys. **95**, 4877 (1991).
[35]T. Glenewinkel-Meyer and D. Gerlich, Isr. J. Chem. **37**, 343 (1997).
[36]C. W. Eaker and G. C. Schatz, J. Phys. Chem. **89**, 2612 (1985).
[37]J. K. Badenhoop, G. C. Schatz, and C. W. Eaker, J. Chem. Phys. **87**, 5317 (1987).
[38]J. R. Stine and J. T. Muckerman, J. Chem. Phys. **68**, 185 (1978).
[39]F. Calvo, F. Y. Naumkin, and D. J. Wales, J. Chem. Phys. **135**, 124308 (2011).
[40]F. Calvo, F. Y. Naumkin, and D. J. Wales, Chem. Phys. Lett. **551**, 38 (2012).
[41]F. Y. Naumkin and D. J. Wales, Mol. Phys. **93**, 633 (1998).
[42]N. L. Doltsinis, P. J. Knowles, and F. Y. Naumkin, Mol. Phys. **96**, 749 (1999).
[43]F. Y. Naumkin and D. J. Wales, Mol. Phys. **96**, 1295 (1999).
[44]R. K. Preston and J. C. Tully, J. Chem. Phys. **54**, 4297 (1971).
[45]A. Aguado and M. Paniagua, J. Chem. Phys. **96**, 1265 (1992).
[46]A. Aguado, C. Suarez, and M. Paniagua, J. Chem. Phys. **101**, 4004 (1994).
[47]C. Sanz, O. Roncero, C. Tablero, A. Aguado, and M. Paniagua, J. Chem. Phys. **114**, 2182 (2001).
[48]C. Leforestier, R. H. Bisseling, C. Cerjan, M. D. Feit, R. Friesner, A. Guldberg, A. Hammerich, G. Jolicard, W. Karrlein, H. D. Meyer, N. Lipkin, O. Roncero, and R. Kosloff, J. Comput. Phys. **94**, 59 (1991).

Reuse of AIP Publishing content is subject to the terms: https://publishing.aip.org/authors/rights-and-permissions. Downloaded to IP: 161.111.22.69 On: Thu, 04 Aug 2016 09:50:28

[49]L. F. Shampine and M. K. Gordon, DDEABM is a driver for a modification of the code ODE written by L. F. Shampine and M. K. Gordon, Sandia Laboratories Albuquerque, New Mexico 87185.
[50]M. Karplus, R. N. Porter, and R. D. Sharma, J. Chem. Phys. **43**, 3259 (1965).
[51]H.-J. Werner, P. J. Knowles, J. Almlöf, R. D. Amos, A. Berning *et al.*, MOLPRO, version 2012.1, a package of *ab initio* programs, 2012, see http://www.molpro.net.
[52]J. D. Shao and C. Y. Ng, J. Chem. Phys. **84**, 4317 (1986).
[53]M. Baer and C. Y. Ng, J. Chem. Phys. **93**, 7787 (1990).
[54]R. D. Levine and R. B. Bernstein, *Molecular Reaction Dynamics and Chemical Reactivity* (Oxford University Press, 1987).
[55]J. D. Burley, K. M. Ervin, and P. B. Armentrout, Int. J. Mass Spectrom. Ion Processes **80**, 153 (1987).
[56]S. Gómez-Carrasco, B. Godard, F. Lique, N. Bulut, J. Klos, O. Roncero, A. Aguado, F. J. Aoiz, M. Etxaluze, J. F. Castillo, J. R. Goicoechea, and J. Cernicharo, Astrophys. J. **794**, 33 (2014).
[57]G. E. Moyano, D. Pearson, and M. A. Collins, J. Chem. Phys. **121**, 12396 (2004).
[58]A. Alijah and A. J. C. Varandas, J. Chem. Phys. **129**, 034303 (2008).

Reuse of AIP Publishing content is subject to the terms: https://publishing.aip.org/authors/rights-and-permissions. Downloaded to IP: 161.111.22.69 On: Thu, 04 Aug 2016 09:50:28